SCOPE11 Method for Estimating Aircraft Black Carbon Mass and Particle Number Emissions

SCOPE11 Method for Estimating Aircraft Black Carbon Mass and Particle Number Emissions

Akshat Agarwal[†], Raymond L. Speth[†]*, Thibaud M. Fritz[†], S. Daniel Jacob[‡], Theo Rindlisbacher[§], Ralph Iovinelli[‡], Bethan Owen[¥], Richard Miake-Lye[¶], Jayant S. Sabnis[†], Steven R. H. Barrett[†]

[†]Laboratory for Aviation and the Environment, Department of Aeronautics and Astronautics, Massachusetts Institute of Technology, Cambridge, MA, 02140, United States

[‡]Federal Aviation Administration, Office of Environment and Energy, Washington, DC, 20591, United States

[§]Swiss Federal Office of Civil Aviation, CH-3003 Bern, Switzerland

[¥]Manchester Metropolitan University, Manchester, M15 6BH, United Kingdom

[¶]Aerodyne Research, Inc., Billerica, MA, 01821, United States

ABSTRACT

Black carbon (BC) emissions from aircraft engines lead to an increase in the atmospheric burden of fine particulate matter ($PM_{2.5}$). Exposure to $PM_{2.5}$ from sources including aviation is associated with an increased risk of premature mortality, and BC suspended in the atmosphere has a warming impact on the climate. BC particles emitted from aircraft also serve as nuclei for contrail ice particles, which are a major component of aviation's climate impact. In order to facilitate the

evaluation of these impacts, we have developed a method to estimate BC mass and number emissions at the engine exit plane, referred to as the Smoke Correlation for Particle Emissions – CAEP11 (SCOPE11). We use a dataset consisting of SN – BC mass concentration pairs, collected using certification-compliant measurement systems, to develop a new relationship between Smoke Number (SN) and BC mass concentration. In addition, we use a complementary dataset to estimate measurement system loss correction factors and particle geometric mean diameters to estimate BC number emissions at the engine exit plane. Using this method, we estimate global BC emissions from aircraft landing and takeoff (LTO) operations for 2015 to be 0.74 Gg/yr (95% CI: 0.64 – 0.84) and 2.85×10^{25} particles/yr (95% CI: $1.86 - 4.49 \times 10^{25}$).

TOC ART

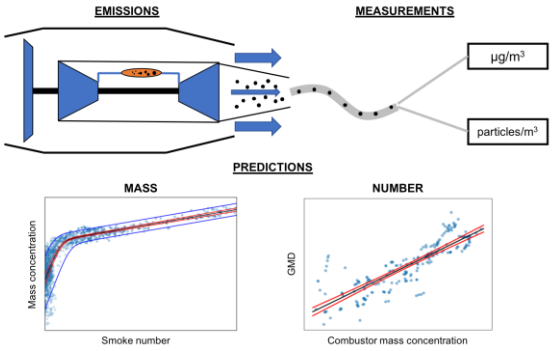

INTRODUCTION

Global commercial aviation activity is expected to grow by 1.5-4.1% annually between 2020 and 2050 under a range of IPCC scenarios (1). The upper side of this range is consistent with industry projections that expect requiring almost double the fleet size by 2036 (2,3). Emissions from aircraft engines near airports can increase particulate matter (PM) and ozone (O_3) concentrations (4,5). The inhalation of fine PM with an aerodynamic diameter below 2.5 μm

($PM_{2.5}$) by surrounding populations can lead to adverse health impacts and an increase in premature mortalities (6,7).

While current epidemiological evidence is based on mass concentrations, increasing toxicological evidence points to the importance of number (or surface area) as a metric of importance (8). This is a particular concern for aviation engines due to their capacity to produce so-called "ultra-fine" particulate matter, with aerodynamic diameter below 100 nm (9–14). Emissions of these ultra-fine particles can lead to a significant increase in ambient particle number concentrations, with decreases in average particle size, leading to increased lung deposition fractions (15–18). The air quality and health impacts from aviation emissions have been quantified at scales spanning airport and regional level calculations (19–22) to national level estimates (5,23,24) to global aviation activity (4,25,26). Median estimates for premature mortalities attributable to all aviation emissions in 2006 vary between 9,000 (25) and 16,000 (4), which represents $\lesssim$ 2% of premature mortalities caused by outdoor air quality degradation due to anthropogenic emissions. BC emissions account for ~0.2% of this health impact due to full flight, global emissions (27). However, this result does not account for differences between fine and ultra-fine PM, and the BC contribution may be higher at a regional level (5). In addition, BC particles emitted at cruise altitudes serve as ice nuclei to promote the formation of contrails. Contrails are considered to be one of the largest of aviation's climate impacts (28,29) and have been found to be sensitive to BC number emissions (30,31).

These concerns have led the International Civil Aviation Organization's (ICAO) Committee for Aviation Environmental Protection (CAEP) to develop emissions standards for aircraft engines, which currently include limits on NO_x, unburned hydrocarbons, and carbon monoxide emissions during a standard landing and takeoff (LTO) cycle (32). Aircraft engine black carbon (BC)

emissions have also been regulated indirectly through the Smoke Number (SN) standard adopted in 1981.

The SN standard was developed to limit the visibility of the black soot from aircraft engine exhaust plumes. It is measured by capturing the BC in the exhaust stream on a filter and measuring its change in reflectance (33). While the SN is useful for estimating the visibility of the plume, it is not a suitable metric to quantify air quality impacts on human health. Advanced measurement systems have therefore been developed to measure BC emissions from aircraft engines. The systems have evolved over a series of engine measurement campaigns, including the Aircraft Particle Emissions Experiment (APEX) (34), the Aviation-Particulate Regulatory Instrumentation Demonstration Experiment (A-PRIDE) (9), and an additional study demonstrating the method for smaller engines (10). This work has culminated in an Aerospace Recommended Practice (ARP) that provides guidelines for the measurement of BC emissions (35).

In addition to improvements in the measurement systems, reporting requirements and a mass concentration standard for engines produced after 1 January 2020 were established at the 10th meeting of CAEP. While this reporting requirement is useful for quantifying future emissions of BC mass and number, there remain a range of engines that are expected to continue active operation with no BC measurements available. For this reason, various correlations have been developed that relate SN with BC mass concentration, including the FOA3 method (36) and a correlation developed by Stettler et al. (37). These have been used as the basis of estimates for several air quality studies, however they can vary by a factor of 4 in estimating total global BC emissions (38). To the best of the authors' knowledge, no relationships exist to predict BC number emissions from engine certification data, except for using simplified relationships that are extremely sensitive to the choice of a constant geometric mean diameter (GMDs).

In this paper, we use a dataset of simultaneous SN and mass concentration measurements to improve the estimation of aircraft engine BC mass concentration from SN data (dataset-1). While similar in form to the original dataset used to develop FOA3 (36), the measurements used here were taken using a standardized measurement system defined in ICAO Annex 16 Vol. II (32) and the SN and mass concentration measurements were acquired simultaneously. The FOA3 method was developed using certification SN data, with mass concentration measured independently using in-service engines. Thus, dataset-1 is expected to lead to a more reliable correlation than these previous studies. Despite the advancements in measurement systems, the long sampling lines required to transport the BC from engine exit to measurement devices lead to particle losses as, for example, particles are deposited on the walls of the sampling lines. These losses have been discussed in various measurement campaigns (11,34) and can be in excess of 50%, increasing as the geometric mean diameter (GMD) of particles decreases (39). Using a dataset of simultaneous BC mass and particle number emissions (dataset-2), we have developed a correlation to estimate mass system loss correction factors when only mass concentration data is available. Using this same dataset, we have developed a method to predict BC number emissions by assuming a lognormal size distribution and correlating the GMD with a function of measured mass concentration and the pressure at the combustor exit. These correlations and the method to convert them to total BC mass and number emissions is referred to as the Smoke COrrelation for Particle Emissions – CAEP11 (SCOPE11), and will be used by airports and ICAO-CAEP in developing international standards for the regulation of aircraft engine BC emissions. In addition, this work can be used by modelers to improve estimates for aviation BC emissions and evaluations of aviation's environmental impact.

MATERIALS AND METHODS

SN to BC mass concentration correlation: We use a dataset of 1407 paired BC mass concentration (C_{BC}) and SN measurements referred to as dataset-1. These measurements were taken in order to support the CAEP process, and comprise measurements of 24 aircraft engine models from 6 manufacturers over a range of engine thrust settings. The SN and C_{BC} measurements were made using standardized measurement systems as defined in ICAO Annex 16 Vol. II (32) and the data represents measurements at the instrument ($C_{BC,i}$), rather than at the engine exit plane ($C_{BC,e}$), but does include corrections for thermophoretic losses (32,33). The measurement system involves three sections: collection, transfer and measurement. The collection of BC particles occurs through a single- or multi-point rake with sampling probes, after which the sample flows through a heated sample line. The sample is then transferred to a diluter to reduce further coagulation and thermophoretic losses, before being passed through a 1 μm cyclone separator in order to remove large particles that are assumed not to be generated by combustion. Finally, BC mass measurements are made using either an AVL Micro Soot Sensor (MSS) or Laser Induced Incandescence (LII), and number measurements are made using an AVL Particle Counter (APC), which also requires a volatile particle remover (VPR) to condition the sample for non-volatile particle number measurements. Major sources of uncertainty are found in the measurement instruments, estimated to be ~25% for both mass and number, as well as errors due to temperature and pressure measurements, and errors due to dilution factor measurements (9).

By using standardized, certification-compliant measurement systems, dataset-1 contains high quality measured data from a wide variety of engines, which has previously been unavailable. This data has been included in the Supplementary Information (SI) Document B, with additional information removed to respect proprietary concerns for each manufacturer. The measurement

points are shown in**Error! Reference source not found.** Figure 1 (blue circles). We note that while the data has a general exponential trend for SN $\gtrsim 5$ (linear in semi-logarithmic axes), the behavior below this SN is not as clear. In the SN < 5 regime, there is significant spread in the data, such that at SN = 0, the $C_{BC,i}$ can vary by approximately 3 orders of magnitude. To help visualize the trends, we have separated the data into 25 distinct bins by range of SN and plotted the median mass concentration for each bin (orange, unfilled circles). The median set of data reveals an exponential trend for SN $\lesssim 5$ that has a steeper gradient than that for higher SNs.

To account for the observed shape and the changing trend between low and high SN, we develop a correlation using the product of an exponential function (governing the behavior for high SN) and a logistic function (governing the behavior for low SN):

$$C_{BC,i} = \frac{k_1 e^{k_2 \mathrm{SN}}}{1 + e^{k_3(\mathrm{SN}+k_4)}} \qquad \text{Eq 1}$$

where k_i are constants that are determined by a two-step nonlinear least-squares fit. In each step, the fit is carried out on the logarithm of $C_{BC,i}$ in order to produce a fit that is applicable across the full range of SNs. In the first step, the constants k_1 and k_2 are found by fitting the data for SN ≥ 5 to the exponential function $C_{BC,i} = k_1 e^{k_2 \cdot \mathrm{SN}}$. In the second step, the full data set is fit to the combined equation, holding k_1 and k_2 constant, in order to find k_3 and k_4.

To quantify the variability within the data, we also calculate prediction intervals. These are the intervals between which we have a specified probability (e.g. 90%) that a new concurrent SN and $C_{BC,i}$ measurement would lie. To determine these bounds, we hold k_2 and k_3 fixed. k_1 is found using an optimization routine that uses the SN ≥ 5 data and ensures 5% of the data above and 5% of the data below the upper and lower bounding lines respectively. The same method is used to find k_4, but using the data for SN ≤ 5.

System loss corrections: As with any sampling-based particle measurement, there are particle losses in the standardized measurement system which lead to differences between the BC emissions measured at the instruments versus those actually emitted from the engine at the exit plane. Losses occur due to changes in flow direction that cause particles to embed on internal surfaces. This loss can occur due to bends in the sampling lines and the lack of penetration of particles through individual components. The losses of particles in individual components can also be a function of size. For example, losses in the VPR are determined to be around 60% for particles with 15 nm aerodynamic diameter, and 30% at a diameter of 50 nm (10), consistent with trends from measurements for automotive vehicle emissions (40). These losses, referred to as system losses, have been found to reduce the measured mass of emissions by up to a factor of 2, while losses for number emissions can be greater than a factor of 50 (39). Losses depends on particle size due to device-specific penetration functions and the higher diffusion of smaller particles that can be absorbed on the line walls. These losses can be estimated by using a system loss calculator developed by SAE (39), which requires input on the exhaust gas temperature, sampling line lengths and temperatures, and measured values.

Given that dataset-1 contains measurements at the instrument, we must correct for system losses to estimate emissions at the engine exit plane. Using a set of simultaneous BC mass and particle number data measured using the standard-compliant measurement systems (41) (dataset-2) and corrected for differences in fuel hydrogen content, system loss correction factors for mass (k_{slm}) have been estimated using the SAE system loss calculator (39). We observe that the mean particle size, or the geometric mean diameter (GMD), tends to increase with increasing combustor mass concentration due to coagulation (see subsequent subsections) and thus can be used to predict k_{slm}. To allow for a closed-form equation for k_{slm}, we use the mass

concentration per unit volume of core flow at the instrument, which has also been found to be a good predictor of the GMD and thus k_{slm}. This dataset contains 264 measurements and has also been included in SI Document B, again with additional data removed to protect the identity of specific engines or manufacturers.

The system loss correction factors have been correlated with BC mass concentration using the functional form:

$$k_{slm} = \ln\left(\frac{a_1 \cdot C_{BC,i}(1+\beta_{mix}) + a_2}{C_{BC,i}(1+\beta_{mix}) + a_3}\right) \quad \text{Eq 2}$$

where β_{mix} is equal to the bypass ratio for mixed-flow engines and zero otherwise. The factor $1+\beta_{mix}$ corrects the exit plane mass concentration for mixed-flow engines to a core-equivalent value. The form of the equation was chosen to obtain the expected asymptotic behavior at high mass concentrations or high GMDs ($k_{slm} \to \ln a_1$) and a bounded value at low concentrations or low GMDs ($k_{slm} = \ln\frac{a_2}{a_3}$).

The fit is conducted using non-linear regression, with 34 of the data points discarded as they were either below the mass measurement limit of detection ($C_{BC,lim} = 1.0\ \mu g/m^3$), were considered anomalous due to measurement errors, or system loss correction data was not available. k_{slm} can be applied as a multiplicative factor on the emissions index for the mass of BC, $EI_{m,i}(BC)$, which measures the mass of BC produced per mass of fuel burnt [mg/kg-fuel]. We use the Python package Kapteyn (42), which uses a linear approximation of Eq 2 to estimate the confidence and prediction intervals. To prevent unrealistic values, we constrain the intervals to have a value greater than or equal to 1.

Calculating Emissions Indices: Using the SCOPE11 correlation, we can estimate C_{BC} from SN data. This can be converted into an emissions index following the method described by

Wayson et al. (36). $EI_{m,i}(BC)$ is calculated by multiplying $C_{BC,i}$ with the volumetric flow rate, Q [m^3/kg-fuel]. By assuming a fuel hydrogen content of 13.8% by mass, this is calculated as:

$$Q_{\text{unmixed}} = 0.776 \cdot \text{AFR} + 0.767$$
$$Q_{\text{mixed}} = 0.776 \cdot \text{AFR} \cdot (1 + \beta) + 0.767 \quad \text{Eq 3}$$

where, Q_{unmixed} is the volumetric flow rate for engines with an unmixed exhaust nozzle and Q_{mixed} is for engines with mixed nozzles that require a correction for the bypass ratio, β. These equations require an estimate of the overall air to fuel ratio (AFR). Wayson et al. (36) provide estimates for AFR at the four ICAO LTO thrust settings of 106 at idle, 83 at approach, 51 at climb-out and 45 at take-off. We then apply the system loss correction factors to $EI_{m,i}(BC)$ to estimate the emissions at the engine exit plane.

Estimating exit plane BC number emissions. The BC number emissions index at the engine exit plane, $EI_{N,e}(BC)$, can be calculated using $EI_{m,e}(BC)$ and an estimate of the geometric mean diameter (GMD) at the same plane. Assuming a log-normal size distribution, the relationship between these variables can be shown to be (43):

$$EI_{N,e}(BC) = \frac{6EI_{m,e}(BC)}{\pi\rho\text{GMD}^3 e^{4.5(ln\sigma)^2}} \quad \text{Eq 4}$$

where ρ is the effective density of soot assumed to be 1000 kg/m^3 and σ is the geometric standard deviation (GSD), which has been found to be ~1.8 from experimental observations (12,44).

In order to apply this equation, we require an estimate for the GMD at the engine exit plane. This value is a complex function of production rates in the combustor primary zone, oxidation of BC in the secondary zone and coagulation of particles as they grow downstream of these regions. Measurement campaigns have also shown that the GMD tends to increase with thrust rating (27,29), which is due in part to the increase in pressure (and therefore density) at higher relative

thrust that drives coagulation rates. As such, we use a measure of the BC mass concentration at the combustor exit, $C_{BC,c}$, which is a function of both $C_{BC,e}$ and the conditions at the combustor exit.

The data required for this correlation is estimated from measurements in dataset-2. The $C_{BC,e}$ is found by converting the $EI_{m,e}(BC)$ in dataset-2 to a concentration using the volumetric flow rate calculated via Eq 3. The exit plane concentration is converted to an estimate of $C_{BC,c}$ using the method outlined below. The GMD at the engine exit plane is then estimated using Eq 4. This first requires converting instrument measured mass and number emission indices to exit plane values. The loss correction factor for mass emissions ranges between 1.1 and 2.4 and that for number between 1.3 and 20.7. Finally, we assume an effective soot density of 1000 kg/m^3 and GSD of 1.8. Using dataset-2, we have developed a correlation of the form:

$$\mathrm{GMD} = a \cdot C_{BC,c}^{b} \qquad \text{Eq 5}$$

where a and b are constants to be determined. $C_{BC,e}$ is scaled to the concentration at the combustor exit using the ratio of the combustor exit to ambient density:

$$C_{BC,c} = C_{BC,e}(1 + \beta_{mix})\frac{\rho_{t4}}{\rho_a} \qquad \text{Eq 6}$$

where $C_{BC,c}$ is the predicted BC mass concentration at the combustor exit, $C_{BC,e}$ is the mass concentration at the engine exit plane, scaled to standard temperature and pressure, β_{mix} is the same parameter as used in Eq 2, ρ_a is the density of ambient air (1.2 kg/m^3) and ρ_{t4} is the total density of air at the combustor exit. ρ_{t4} is dependent on the pressure at the combustor exit, increasing with the thrust level, and can be found using the ideal gas law:

$$\rho_{t4} = \frac{P_{t4}}{R_{\mathrm{air}} T_{t4}} \qquad \text{Eq 7}$$

where subscript $t4$ represents the turbine inlet/combustor exit location, P is the pressure, T is the temperature and R_{air} the specific gas constant of air. The pressure and temperature at the turbine inlet can be estimated by assuming no pressure loss in the combustor and using a first order energy balance across the combustor.

$$P_{t4} = P_{t2}\left(1 + (\pi_{00} - 1)\frac{F}{F_{00}}\right)$$
$$T_{t4} = \frac{\mathrm{AFR}\, c_{p,a}\, T_{t3} + \mathrm{LCV}}{c_{p,e}(1 + \mathrm{AFR})} \qquad \text{Eq 8}$$

where π_{00} is the overall pressure ratio in the engine at rated thrust, F/F_{00} is the fractional thrust, AFR is the air to fuel ratio, $c_{p,a} = 1.005$ kJ/kg/K is the heat capacity at constant pressure of air and $c_{p,e} = 1.250$ kJ/kg/K is that for the combustion products, LCV$= 43.2$ MJ/kg is the lower calorific value of the fuel and T_{t3} is the temperature at the inlet to the combustor. T_{t3} can be estimated assuming a constant polytropic efficiency, η_p, of 0.9 for the flow through the core fan and compressor:

$$T_{t3} = T_{t2}\left(\frac{P_{t3}}{P_{t2}}\right)^{\gamma-1/\gamma\eta_p} \qquad \text{Eq 9}$$

where T_{t2} and P_{t2} are the total temperature and pressure at inlet to the gas turbine and γ is the heat capacity ratio of air (taken to be 1.4). Using these relationships, we can find the BC mass concentration at the combustor exit and subsequently conduct a linear regression on the logarithm of Eq 5. The regression was conducted using the Statsmodel package in Python (45), which also estimate the confidence and prediction intervals. When conducting the regression, we discard the same data points that were discarded in the regression conducted for system loss corrections.

Estimating global LTO BC emissions: LTO BC emissions for commercial, passenger aviation activity in 2005 and 2015 can be estimated directly from the number of aircraft operations and the type of aircraft for each origin-destination pair. The Official Airline Guide (OAG) supplies schedule data with information on airport pairs that includes both sets of information for a full year. Matching the aircraft to an engine allows us to estimate SN and fuel flow rates by identifying the engine in the ICAO engine emissions database (46). This can be used with the ICAO LTO cycle (32), reflective of aircraft operations up to 915 m above ground level, and the correlations for $EI_m(BC)$, k_{slm} and $EI_N(BC)$ developed in this paper to calculate the exit-plane mass and number of BC emissions for a specified aircraft engine. Further details on the OAG data and aircraft-engine pairs can be found in Stettler et al. (24).

Propagating uncertainties: For all the correlations that have been conducted, we include confidence and prediction intervals. Confidence intervals provide the range between which the true regression line is expected to be found with probability $(1 - \alpha_c)$. This informs us on the uncertainty in estimating the mean results. Prediction intervals provides the range between which an individual observation may lie with probability $(1 - \alpha_p)$. This interval includes the uncertainty in the mean result, as in confidence intervals, as well as the scatter in the underlying data, leading to a wider interval. These two intervals encompass the uncertainties inherent in all of the methods. For example, in the SN to $C_{BC,i}$ correlation, the uncertainty increases as the SN decreases. For k_{slm}, differences between measurement systems and their setup and calibration can lead to variations in the mass system loss correction. Finally, the GMD to $C_{BC,c}$ correlation relies on assumptions on the effective soot density and GSD. Given sufficient data, all of these uncertainties as well as the underlying measurement uncertainties will be reflected in the variation of the

measurements around the best fit line. In turn, this variability is accounted for in the confidence and prediction intervals.

The confidence intervals can be used to estimate the uncertainty in the global LTO BC estimates. We apply the lower and upper confidence intervals for each correlation to get a lower and upper estimate of the uncertainty in the global LTO BC estimates. The prediction intervals can be used to estimate the uncertainty in individual predictions of $EI_{m,i}(BC)$, $EI_{m,e}(BC)$ and $EI_{N,e}(BC)$, as shown in SI Document A.

RESULTS

SN to $C_{BC,i}$ correlation: The two step, nonlinear least squares fit leads to the following best fit relationship:

$$C_{BC,i}\left[\frac{\mu g}{m^3}\right] = \frac{648.4\, e^{0.0766 \cdot SN}}{1 + e^{-1.098 \cdot (SN - 3.064)}} \quad \text{Eq 10}$$

This is shown by the black, solid line in Figure 1. The 95% confidence intervals in the parameters are

$$\begin{aligned} k_1 &= 648.4 \pm 44.9\ \mu g/m^3 \\ k_2 &= 0.0766 \pm 0.0038 \\ k_3 &= -1.098 \pm 0.120 \\ k_4 &= -3.064 \pm 0.277 \end{aligned} \quad \text{Eq 11}$$

The prediction intervals within which future measurements would lie with 90% probability is also found using a similar two-step method. The resulting intervals are

Lower:

$$C_{BC,i}\left[\frac{\mu g}{m^3}\right] = \frac{378.5\, e^{0.0766 \cdot SN}}{1 + e^{-1.098 \cdot (SN - 5.066)}} \quad \text{Eq 12}$$

Upper:

$$C_{BC,i}\left[\frac{\mu g}{m^3}\right] = \frac{1146.2\ e^{0.0766 \cdot SN}}{1 + e^{-1.098 \cdot (SN - 1.480)}}$$

These equations, along with the best fit line, are shown in Figure 1. The gradients of the high SN and low SN limits are equal for the lower, upper and best fit lines. However, the transition point between these regions moves from 1.480 for the upper line to 5.066 for the lower line.

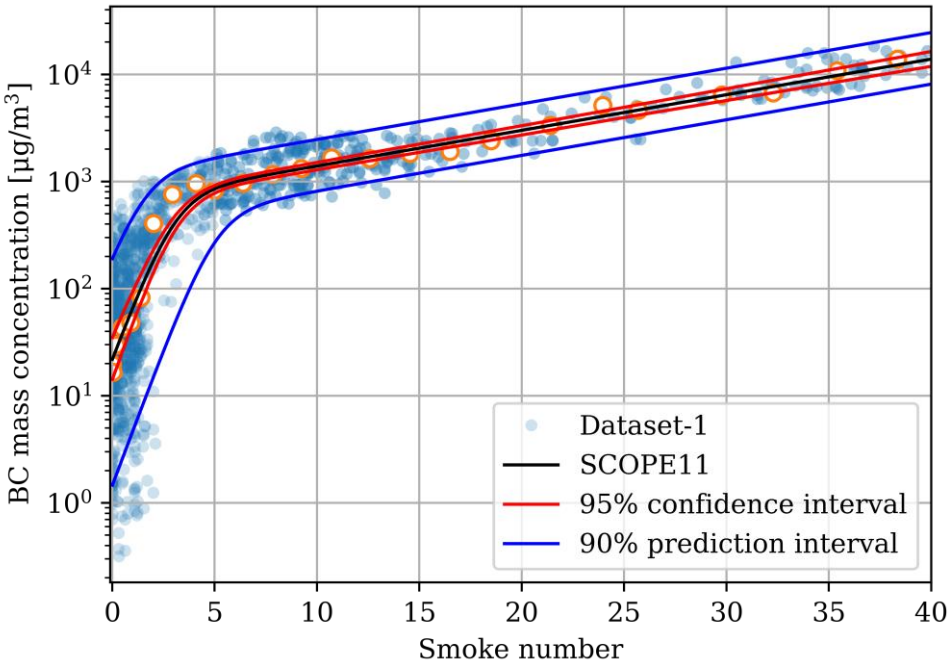

Figure 1: SCOPE11 best fit line (black) with 95% confidence intervals (red) and 90% prediction intervals (blue). The unfilled orange circles represent the median values of binned dataset-1 values.

Figure 2 provides a comparison of the SCOPE11 correlation to the FOA3 (36) and Stettler et al. (37) correlations. The FOA3 relationship (36) was developed using a dataset similar to dataset-1, where the measurements were not taken using a standardized measurement system, which consisted of fewer than 75 points (compared to 1406 data pairs used here), and used SN and mass concentration measurements which were not taken concurrently. Due to these differences, the FOA3 relationship tends to predict lower $C_{BC,i}$ than the SCOPE11 correlation, except at a SN $\approx$ 2 and between 15 and 20. In addition, the FOA3 model assumes that that $C_{BC,i} = 0$ when SN $= 0$,

whereas the data shows a median of $C_{BC,i} = 19.6\ \mu g/m^3$ and a variation spanning 3 orders of magnitude at SN = 0.

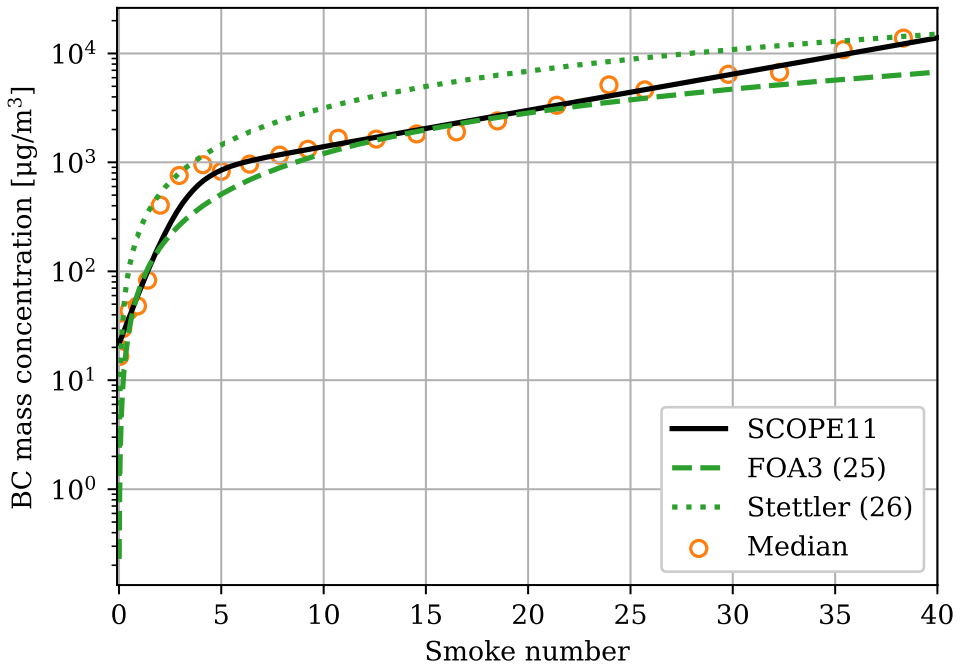

Figure 2: Comparison between SCOPE11 (black), FOA3 (dashed, green line) and the Stettler et al. (26) correlations (dotted, green line).

Stettler et al. (37) used an inverse diffusion flame to generate BC, following a standardized procedure for measuring SN. However, their methods to measure BC mass differ from the certification-compliant system. They developed SN – BC mass concentration relationships for GMDs between 20 and 30 nm and for GMDs of ~60 nm, advising use of the former correlation for aircraft engines. This correlation tends to predict higher mass concentrations for a wide range of SN than the SCOPE11 correlation, lying outside of the range of the data found in dataset-1 for SNs between ~10 and ~25. Stettler et al. (37) also use a functional form which assumes that $C_{BC,i} = 0$ when SN = 0.

System loss corrections. The median relationship to estimate k_{slm} from $C_{BC,i}$ is shown in Eq 13. The 95% confidence intervals for each of the constants is also shown in the set of equations Eq 14.

$$k_{slm} = \ln\left(\frac{3.219 \cdot C_{BC,i}(1+\beta_{mix}) + 312.5}{C_{BC,i}(1+\beta_{mix}) + 42.6}\right) \quad \text{Eq 13}$$

$$\begin{aligned} a_1 &= 3.219 \pm 0.135 \\ a_2 &= 312.5 \pm 119.1\ \mu g/m^3 \\ a_3 &= 42.6 \pm 19.4\ \mu g/m^3 \end{aligned} \quad \text{Eq 14}$$

The results of this fit and the associated data is shown in Figure 3. This functional form predicts that as $C_{BC,i}$ continues to increase, k_{slm} tends towards a constant value of $\sim 1.169 \pm 0.041$. This is analogous to the tendency of k_{slm} to approach a constant value as the GMD increases (39). In addition, for $C_{BC,i}$ tending towards 0, we find $k_{slm} = 1.99$, which is a typical value for GMD $\approx$ 10 nm, the minimum size which the measurement system can reliably capture. The spread in the measurement points are caused by two effects. First, there are differences between the systems used by each manufacturer, permitted within the measurement guidelines. These differences can include, for example, specifications of components such as the VPR, or differences in instrument calibration. Second, variations in the engine exhaust temperature can change the degree of thermophoretic losses that occur along sampling lines, which is estimated via an analytical form, also affecting k_{slm}.

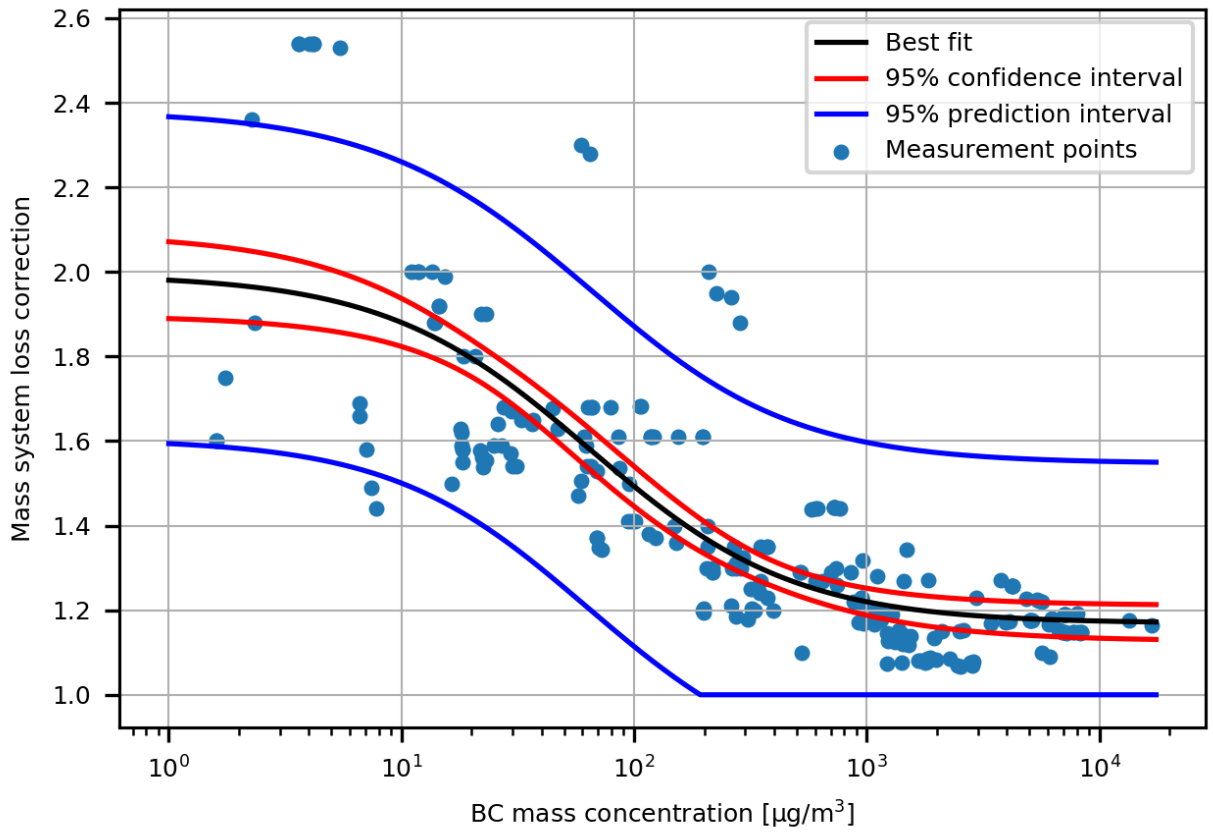

324

325 **Figure 3:** Measured BC mass concentration versus k_{slm} estimated using the line loss calculator.

326 **Exit plane GMD.** The results of the linear least squares regression on the power law relationship
327 between $C_{BC,c}$ (in µg/m^3) and GMD is shown in Eq 15 with associated 95% confidence intervals
328 for each constant in Eq 16.

$$\text{GMD [nm]} = 5.08\ {C_{BC,c}}^{0.185} \qquad \text{Eq 15}$$

$$a = 5.08 \pm 0.55 \text{ nm}$$
$$b = 0.185 \pm 0.015 \qquad \text{Eq 16}$$

The results of this fit and the associated data are shown in Figure 4. The adjusted R-squared was found to be 0.72 and p-values < 0.001. This relationship can thus be used to estimate the $EI_{N,e}(BC)$ using Eq 4.

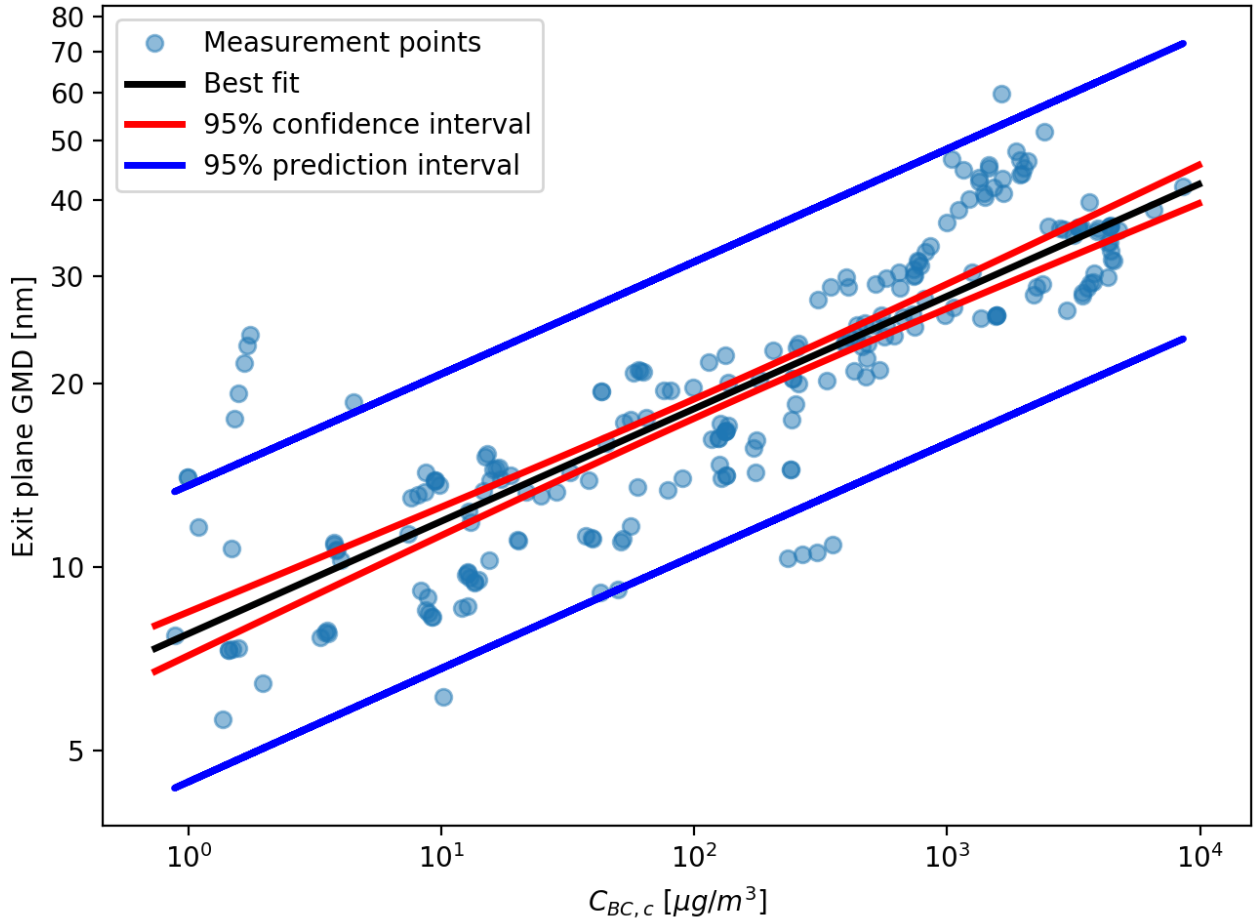

Figure 4: Combustor exit BC mass concentration vs GMD in logarithmic axes

The correlation to predict GMD is dependent on the choice of the effective soot density and GSD. These are both uncertain parameters and we only use estimates of their mean value to produce this correlation. While the choice of these variables is important in estimating the GMD, they are not critical to estimating $EI_{N,e}(BC)$, since the regression constants will vary according to the assumed density and GSD, leading to a similar estimate in the $EI_{N,e}(BC)$ but with a different estimate for the GMD.

340 **Comparison of measured and predicted EI.** Using the results presented in the earlier
341 sections, we can estimate $EI_{m,i}(BC)$, $EI_{m,e}(BC)$ and $EI_{N,e}(BC)$ for engines found in dataset-2,
342 beginning with the SN at each mode of operation. Figure 5 shows the comparisons for $EI_m(BC)$
343 both with (B) and without system loss corrections (A). $EI_N(BC)$ is shown with system loss
344 corrections only (C). The R^2 and root mean square error (RMSE) for each mode of operation as
345 well as overall are shown in Table 1. These values show that the overall R^2 is ~0.8 for all cases,
346 however the values for taxi operations for $EI_{m,i}(BC)$ and $EI_{m,e}(BC)$ tend to be lower than the
347 other modes. RMSE values vary between 62.9 mg/kg-fuel and 74.7 mg/kg-fuel for $EI_{m,i}(BC)$
348 and between 76.4 mg/kg-fuel and 87.6 mg/kg-fuel for $EI_{m,e}(BC)$. Table 1 also includes the R^2
349 and RMSE values when using the FOA3 (36) or Stettler (37) correlation in place of SCOPE11,
350 to estimate $EI_{m,i}(BC)$. While the R^2 values are all similar, our methods tends to produce a higher
351 R^2 than both, except at taxi thrust. The RMSE is lower using the SCOPE11 than the FOA3
352 method for all modes except taxi by 10-15%. The RMSE using the Stettler et al. (37) correlation
353 are 168% larger than using the SCOPE11 method overall, increasing as a function of mode.
354
355 **Table 1:** R^2 and RMSE values for instrument mass emissions index ($EI_{m,i}(BC)$), exit-plane mass
356 emissions index ($EI_{m,e}(BC)$), and exit-plane number emissions index ($EI_{\mathrm{N},e}(BC)$), separated by
357 mode of operation and overall. For the exit-plane mass emissions, the SCOPE11 method is
358 compared to the FOA3 (36) and Stettler et al. (37) methods.

		$EI_{m,i}(BC)$			$EI_{m,e}(BC)$	$EI_{N,e}(BC)$
		SCOPE11	**FOA3 (36)**	**Stettler et al. (37)**	**SCOPE11**	**SCOPE11**
Taxi	**R^2**	0.26	0.35	0.36	0.31	0.77

	RMSE	65 mg/kg	61 mg/kg	102 mg/kg	78 mg/kg	3.1×10^{15} particles/kg
Approach	**R^2**	0.83	0.76	0.78	0.83	0.84
	RMSE	63 mg/kg	73 mg/kg	149 mg/kg	86 mg/kg	2.6×10^{15} particles/kg
Climb-out	**R^2**	0.83	0.79	0.81	0.84	0.89
	RMSE	74 mg/kg	84 mg/kg	224 mg/kg	86 mg/kg	1.8×10^{15} particles/kg
Take-off	**R^2**	0.75	0.73	0.75	0.80	0.85
	RMSE	75 mg/kg	82 mg/kg	249 mg/kg	86 mg/kg	8.2×10^{14} particles/kg
Overall	**R^2**	0.79	0.75	0.76	0.80	0.82
	RMSE	69 mg/kg	75 mg/kg	186 mg/kg	82 mg/kg	1.6×10^{15} particles/kg

359

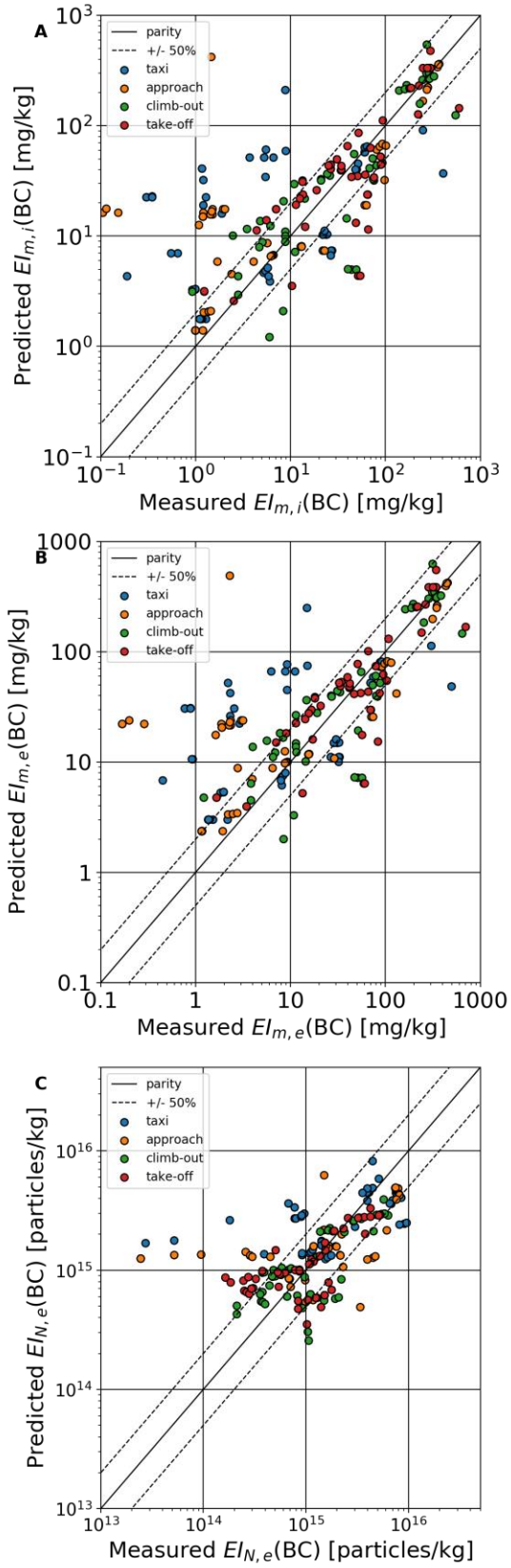
A
parity
+/- 50%
taxi
approach
climb-out
take-off
Predicted $EI_{m,i}$(BC) [mg/kg]
Measured $EI_{m,i}$(BC) [mg/kg]
B
parity
+/- 50%
taxi
approach
climb-out
take-off
Predicted $EI_{m,e}$(BC) [mg/kg]
Measured $EI_{m,e}$(BC) [mg/kg]
C
parity
+/- 50%
taxi
approach
climb-out
take-off
Predicted $EI_{N,e}$(BC) [particles/kg]
Measured $EI_{N,e}$(BC) [particles/kg]

360

Figure 5: Parity plots of predicted versus measured results for (A) $EI_{m,i}(BC)$, (B) $EI_{m,e}(BC)$ and (C) $EI_{\mathrm{N},e}(BC)$. The R^2 in each case are 0.79, 0.80 and 0.82 respectively.

We have also propagated the prediction intervals from each correlation to estimate the prediction intervals for mass and number emission indices, and these results can be found in SI Document A. We find that the uncertainty in $EI_{m,i}(BC)$ tends to decrease as the emissions increase and the uncertainty can span almost 2 orders of magnitude at lower SN. For number emissions, the uncertainty decreases slightly as emissions decrease, however in all cases is large and spans 1-2 orders of magnitude.

Global LTO BC emissions. Estimates of annual emissions of BC due to LTO activity for 2005 and 2015 are presented in Table 2. Using the SCOPE11 correlation, we estimate LTO BC mass emissions to be 0.83 Gg/yr (95% confidence interval (CI): 0.72 – 0.95) in 2005 and 0.74 Gg/yr (95% CI: 0.64 – 0.84) in 2015. We also find LTO BC number emissions to be 3.23×10^{25} particles/yr (95% CI: $2.15 – 5.02 \times 10^{25}$) and 2.85×10^{25} particles/yr (95% CI: $1.86 – 4.49 \times 10^{25}$) in 2005 and 2015, respectively.

Table 2: Comparison of global LTO BC estimates. For SCOPE11-estimated BC mass and number emissions, we include estimates of the 95% confidence intervals in parentheses.

Method	**LTO BC Mass [Gg/yr]**		**Fleet average LTO $EI_m(BC)$ [mg/kg-fuel]**	
	2005	**2015**	**2005**	**2015**
SCOPE11	0.83 (0.72 – 0.95)	0.74 (0.64 – 0.84)	55 (47 – 63)	40 (35 – 46)
FOA3 (36)	0.55	0.51	37	28

Stettler et al. (37)	1.48	1.38	98	75
	LTO BC Number [$\times 10^{25}$ particles/yr]		**Fleet average LTO $EI_{N,e}(BC)$ [$\times 10^{14}$ particles/kg-fuel]**	
SCOPE11	3.23 (2.15 – 5.02)	2.85 (1.86 – 4.49)	21 (14 – 33)	15 (10 – 24)

The difference in annual LTO BC mass emissions between methods shows a similar trend to that found in Figure 1 for the correlation between SN and C_{BC}. The SCOPE11 method predicts ~31% higher BC mass emissions than FOA3 and ~86% lower than the Stettler et al. (37) correlation for 2015, and the trend is similar for 2005. We also find that the fleet-average $\mathrm{EI}_m(\mathrm{BC})$ using the SCOPE11 method is found to lie between the estimates using the other two methods, with similar relative differences for each year.

We also note that SCOPE11-estimated mass emissions decreased by ~11% between 2005 and 2015. The FOA3 (36) and Stettler et al. (37) correlations also predict a decrease in mass emissions of ~7% each. However, the total LTO fuel burn in 2015 was 22% higher than in 2005. This corresponds to a decrease in the fleet average LTO $EI_m(BC)$ of(38) correlation between 23 – 27% from 2005 to 2015. We also notice a similar trend in number emissions, which decrease by ~12% from 2005 to 2015, also reflecting a decrease in fleet average $EI_N(BC)$ of ~29%.

DISCUSSION

The SCOPE11 SN – C_{BC} correlation reduces the error in estimating BC emissions from aircraft engines in comparison to both the FOA3 (36) and Stettler (37) correlations. This improvement stems from the use of (i) a new database of simultaneously-acquired SN and BC mass concentration measurements taken using certification-compliant measurement systems from a representative sample of modern aircraft engines; (ii) a new functional form that better follows the trends between the SN and BC mass concentration relationship at SN $\lesssim 5$; and (iii) a more

complete approach to characterize the prediction uncertainty. In addition, we have extended the method to predict emissions at the engine exit plane, which accounts for measurement system losses. If system losses are not accounted for, LTO BC emissions may be systematically underestimated by ~20%. Given the direct climate and air quality impacts of aviation BC emissions, it is important to account for measurement system losses when developing emissions inventories. We have also developed a method for estimating BC number emissions at the engine exit plane, by assuming a lognormal size distribution and estimating the GMD from a measure of the BC mass concentration at the combustor exit, and applied this to the development of an inventory of LTO number emissions. To the best of our knowledge, this is the first estimate of BC number emissions from global commercial aircraft LTO operations.

In order to quantify and propagate uncertainty, confidence and prediction intervals have been determined for each correlation and are shown in the figures, with numerical values provided in SI Document B. By propagating confidence intervals through the calculation, lower and upper bounds on the mean global LTO BC emissions are determined. These intervals depend not only on the form of the fitting equation, but also on the spread in the underlying data. This spread depends on variables for which information is available and includes uncertainty in inputs and constant parameters such as the SN, effective soot density and GSD that are required to apply the SCOPE11 method. The latter two variables are of particular importance in the number estimation. While variations in the assumed mean values affects the prediction of the GMD, this has only a second-order effect on the $EI_{\mathrm{N},e}(BC)$ as the regression constants would also change if different values of the effective soot density and GSD were used. The uncertainty ranges calculated highlight the limited degree of correlation between SN and BC concentration at lower emission levels, demonstrating the benefit of developing future emissions standards on mass

concentration and particle number bases and that direct measurements should be used for assessment purposes where they are available.

While the focus of this work is on LTO operations, this work could be combined with existing altitude scaling relationships (47), or used in conjunction with results of recent flight measurement campaigns (48) to inform estimates of cruise-altitude BC emissions. Given the infrequent opportunities to collect BC emissions data at cruise altitude, the development of comprehensive, full-flight inventories of BC mass and number emissions must be based on ground-level emissions estimates, such as those provided by the SCOPE11 method. Such inventories are important components which enable the assessment of aviation's environmental impacts. The ability to predict the size distribution of emissions at the engine exit plane, as in the method developed here, is particularly important for understanding the evolution and radiative impact of contrails, and in modeling the indirect effects of BC particles on natural clouds (49), both of which are among the most uncertain of aviation's climate impacts.

AUTHOR INFORMATION

Corresponding Author

*E-mail: speth@mit.edu; phone: +1 617 253 1516

Funding Sources

This work was made possible by funding from the US Federal Aviation Administration (FAA) Office of Environment and Energy under Project 48 of the ASCENT Center of Excellence under grant 13-C-AJFE-MIT Amendment No. 036.

Notes

The authors declare no competing financial interests.

Supporting Information

SI Document A: Derivation of volumetric flow rate, information on measurement data and confidence intervals and the overall calculation procedure for implementation purposes.

SI Document B: Excel spreadsheet containing the raw data used for developing correlations and associated confidence intervals.

ACKNOWLEDGMENT

The authors would like to thank General Electric Company, GE Aviation Business Unit, Honeywell International Inc, Pratt & Whitney, Pratt & Whitney Canada, Rolls-Royce Plc, and SAFRAN-AE for providing the measurement data on which this work is based.

REFERENCES

1. Owen, B., Lee, D. S. & Lim, L. Flying into the Future: Aviation Emissions Scenarios to 2050. *Environ. Sci. Technol.* **44,** 2255–2260 (2010).
2. Airbus. Global market forecast 2017-2036. (2017). at <http://www.airbus.com/aircraft/market/global-market-forecast.html>
3. Boeing. Current market outlook 2017. (2017). at <http://www.boeing.com/commercial/market/current-market-outlook-2017/>
4. Yim, S. H., Lee, G. L., Lee, I. H., Allroggen, F., Ashok, A., Caiazzo, F., Eastham, S. D., Malina, R. & Barrett, S. R. Global, regional and local health impacts of civil aviation emissions. *Environ. Res. Lett.* **10,** 034001 (2015).
5. Ashok, A., Lee, I. H., Arunachalam, S., Waitz, I. A., Yim, S. H. L. & Barrett, S. R. H. Development of a response surface model of aviation's air quality impacts in the United States. *Atmos. Environ.* **77,** 445–452 (2013).

6. US EPA. The Benefits and Costs of the Clean Air Act: 1990 to 2020 Final report of US Environmental Protection Agency Office of Air and Radiation. (2011).
7. WHO. Health Risks of Particulate Matter from Long-range Transboundary Air Pollution. (2006). at <http://www.euro.who.int/__data/assets/pdf_file/0006/78657/E88189.pdf>
8. Rückerl Regina, Greven Sonja, Ljungman Petter, Aalto Pasi, Antoniades Charalambos, Bellander Tom, Berglind Niklas, Chrysohoou Christina, Forastiere Francesco, Jacquemin Bénédicte, von Klot Stephanie, Koenig Wolfgang, Küchenhoff Helmut, Lanki Timo, Pekkanen Juha, Perucci Carlo A., Schneider Alexandra, Sunyer Jordi & Peters Annette. Air Pollution and Inflammation (Interleukin-6, C-Reactive Protein, Fibrinogen) in Myocardial Infarction Survivors. *Environ. Health Perspect.* **115,** 1072–1080 (2007).
9. Lobo, P., Durdina, L., Smallwood, G. J., Rindlisbacher, T., Siegerist, F., Black, E. A., Yu, Z., Mensah, A. A., Hagen, D. E., Miake-Lye, R. C., Thomson, K. A., Brem, B. T., Corbin, J. C., Abegglen, M., Sierau, B., Whitefield, P. D. & Wang, J. Measurement of Aircraft Engine Non-Volatile PM Emissions: Results of the Aviation-Particle Regulatory Instrumentation Demonstration Experiment (A-PRIDE) 4 Campaign. *Aerosol Sci. Technol.* **49,** 472–484 (2015).
10. Lobo, P., Condevaux, J., Yu, Z., Kuhlmann, J., Hagen, D. E., Miake-Lye, R. C., Whitefield, P. D. & Raper, D. W. Demonstration of a Regulatory Method for Aircraft Engine Nonvolatile PM Emissions Measurements with Conventional and Isoparaffinic Kerosene fuels. *Energy Fuels* **30,** 7770–7777 (2016).
11. Bulzan, D., Anderson, B., Wey, C., Howard, R., Winstead, E., Beyersdorf, A., Corporan, E., DeWitt, M. J., Klingshirn, C., Herndon, S., Miake-Lye, R., Timko, M., Wood, E., Tacina, K. M., Liscinsky, D., Hagen, D., Lobo, P. & Whitefield, P. Gaseous and Particulate Emissions

Results of the NASA Alternative Aviation Fuel Experiment (AAFEX). 1195–1207 (2010). doi:10.1115/GT2010-23524

12. Lobo, P., Hagen, D. E., Whitefield, P. D. & Raper, D. PM emissions measurements of in-service commercial aircraft engines during the Delta-Atlanta Hartsfield Study. *Atmos. Environ.* **104,** 237–245 (2015).
13. Abegglen, M., Durdina, L., Brem, B. T., Wang, J., Rindlisbacher, T., Corbin, J. C., Lohmann, U. & Sierau, B. Effective density and mass–mobility exponents of particulate matter in aircraft turbine exhaust: Dependence on engine thrust and particle size. *J. Aerosol Sci.* **88,** 135–147 (2015).
14. Timko, M. T., Onasch, T. B., Northway, M. J., Jayne, J. T., Canagaratna, M. R., Herndon, S. C., Wood, E. C., Miake-Lye, R. C. & Knighton, W. B. Gas Turbine Engine Emissions—Part II: Chemical Properties of Particulate Matter. *J. Eng. Gas Turbines Power* **132,** 061505-061505–15 (2010).
15. Hudda, N., Gould, T., Hartin, K., Larson, T. V. & Fruin, S. A. Emissions from an International Airport Increase Particle Number Concentrations 4-fold at 10 km Downwind. *Environ. Sci. Technol.* **48,** 6628–6635 (2014).
16. Hudda, N. & Fruin, S. A. International Airport Impacts to Air Quality: Size and Related Properties of Large Increases in Ultrafine Particle Number Concentrations. *Environ. Sci. Technol.* **50,** 3362–3370 (2016).
17. Hudda, N., Simon, M. C., Zamore, W. & Durant, J. L. Aviation-Related Impacts on Ultrafine Particle Number Concentrations Outside and Inside Residences near an Airport. *Environ. Sci. Technol.* **52,** 1765–1772 (2018).

18. Keuken, M. P., Moerman, M., Zandveld, P., Henzing, J. S. & Hoek, G. Total and size-resolved particle number and black carbon concentrations in urban areas near Schiphol airport (the Netherlands). *Atmos. Environ.* **104,** 132–142 (2015).
19. Hsu, H.-H., Adamkiewicz, G., Andres Houseman, E., Vallarino, J., Melly, S. J., Wayson, R. L., Spengler, J. D. & Levy, J. I. The relationship between aviation activities and ultrafine particulate matter concentrations near a mid-sized airport. *Atmos. Environ.* **50,** 328–337 (2012).
20. Unal, A., Hu, Y., Chang, M. E., Talat Odman, M. & Russell, A. G. Airport related emissions and impacts on air quality: Application to the Atlanta International Airport. *Atmos. Environ.* **39,** 5787–5798 (2005).
21. Westerdahl, D., Fruin, S. A., Fine, P. L. & Sioutas, C. The Los Angeles International Airport as a source of ultrafine particles and other pollutants to nearby communities. *Atmos. Environ.* **42,** 3143–3155 (2008).
22. Dodson, R. E., Andres Houseman, E., Morin, B. & Levy, J. I. An analysis of continuous black carbon concentrations in proximity to an airport and major roadways. *Atmos. Environ.* **43,** 3764–3773 (2009).
23. Woody, M., Haeng Baek, B., Adelman, Z., Omary, M., Fat Lam, Y., Jason West, J. & Arunachalam, S. An assessment of Aviation's contribution to current and future fine particulate matter in the United States. *Atmos. Environ.* **45,** 3424–3433 (2011).
24. Stettler, M. E. J., Eastham, S. & Barrett, S. R. H. Air quality and public health impacts of UK airports. Part I: Emissions. *Atmos. Environ.* **45,** 5415–5424 (2011).
25. Barrett, S. R. H., Britter, R. E. & Waitz, I. A. Global Mortality Attributable to Aircraft Cruise Emissions. *Environ. Sci. Technol.* **44,** 7736–7742 (2010).

26. Barrett, S. R. H., Yim, S. H. L., Gilmore, C. K., Murray, L. T., Kuhn, S. R., Tai, A. P. K., Yantosca, R. M., Byun, D. W., Ngan, F., Li, X., Levy, J. I., Ashok, A., Koo, J., Wong, H. M., Dessens, O., Balasubramanian, S., Fleming, G. G., Pearlson, M. N., Wollersheim, C., Malina, R., Arunachalam, S., Binkowski, F. S., Leibensperger, E. M., Jacob, D. J., Hileman, J. I. & Waitz, I. A. Public Health, Climate, and Economic Impacts of Desulfurizing Jet Fuel. *Environ. Sci. Technol.* **46,** 4275–4282 (2012).
27. Koo, J., Wang, Q., Henze, D. K., Waitz, I. A. & Barrett, S. R. H. Spatial sensitivities of human health risk to intercontinental and high-altitude pollution. *Atmos. Environ.* **71,** 140–147 (2013).
28. Lee, D. S., Fahey, D. W., Forster, P. M., Newton, P. J., Wit, R. C. N., Lim, L. L., Owen, B. & Sausen, R. Aviation and global climate change in the 21st century. *Atmos. Environ.* **43,** 3520–3537 (2009).
29. Dorbian, C. S., Wolfe, P. J. & Waitz, I. A. Estimating the climate and air quality benefits of aviation fuel and emissions reductions. *Atmos. Environ.* **45,** 2750–2759 (2011).
30. Kärcher B. & Yu F. Role of aircraft soot emissions in contrail formation. *Geophys. Res. Lett.* **36,** (2009).
31. Caiazzo, F., Agarwal, A., Speth, R. L. & Barrett, S. R. H. Impact of biofuels on contrail warming. *Environ. Res. Lett.* **12,** 114013 (2017).
32. ICAO. Annex 16: Environmental protection, vol. II: Aircraft engine emissions third edition. (2008).
33. ARP1179C. Aircraft gas turbine engine exhaust smoke measurement - SAE Aerospace Recommended Practice (ARP1179C). (1993).

554 34. Wey, C. C., Anderson, B. A., Wey, C., Miake-Lye, R. C., Whitefield, P. & Howard, R.
555 Overview on the Aircraft Particle Emissions Experiment (APEX). *J. Propuls. Power* **23,** 898–
556 905 (2007).
557 35. ARP6320. Procedure for the Continuous Sampling and Measurement of Non-Volatile
558 Particulate Matter Emissions from Aircraft Turbine Engines. (2018).
559 36. Wayson, R. L., Fleming, G. G. & Iovinelli, R. Methodology to Estimate Particulate Matter
560 Emissions from Certified Commercial Aircraft Engines. *J. Air Waste Manag. Assoc.* **59,** 91–
561 100 (2009).
562 37. Stettler, M. E. J., Swanson, J. J., Barrett, S. R. H. & Boies, A. M. Updated Correlation Between
563 Aircraft Smoke Number and Black Carbon Concentration. *Aerosol Sci. Technol.* **47,** 1205–
564 1214 (2013).
565 38. Stettler, M. E. J., Boies, A. M., Petzold, A. & Barrett, S. R. H. Global Civil Aviation Black
566 Carbon Emissions. *Environ. Sci. Technol.* **47,** 10397–10404 (2013).
567 39. AIR6504. Procedure for the Calculation of non-volatile Particulate Matter Sampling and
568 Measurement System Penetration Functions and System Loss Correction Factors - SAE
569 Aerospace Information Report 6504 (AIR6504). (2017).
570 40. Giechaskiel, B., Carriero, M., Martini, G., Krasenbrink, A. & Scheder, D. Calibration and
571 Validation of Various Commercial Particle Number Measurement Systems. *SAE Int. J. Fuels*
572 *Lubr.* **2,** 512–530 (2009).
573 41. AIR6241. Procedure for the Continuous Sampling and Measurement of Non-Volatile Particle
574 Emissions from Aircraft Turbine Engines - SAE Aerospace Information Report 6241
575 (AIR6241). (2013).

42. Terlouw, J. P. & Vogelaar, M. G. R. *Kapteyn Package, version 2.3*. (Kapteyn Astronomical Institute, 2015). at <http://www.astro.rug.nl/software/kapteyn/>

43. Heintzenberg, J. Properties of the Log-Normal Particle Size Distribution. *Aerosol Sci. Technol.* **21,** 46–48 (1994).

44. Kinsey, J. S., Dong, Y., Williams, D. C. & Logan, R. Physical characterization of the fine particle emissions from commercial aircraft engines during the Aircraft Particle Emissions eXperiment (APEX) 1–3. *Atmos. Environ.* **44,** 2147–2156 (2010).

45. Seabold, S. & Perktold, J. *Statsmodels: Econometric and statistical modeling with python*. (2010).

46. EASA. ICAO Engine Emissions Databank (EDB) V24. (2017). at <https://www.easa.europa.eu/easa-and-you/environment/icao-aircraft-engine-emissions-databank#revision-of-data>

47. Dopelheuer, A. & Lecht, M. Influence of engine performance on emission characteristics. in *Symp. Appl. Veh. Technol. Pane-Gas Turbine Engine Combust. Emiss. Altern. Fuels Lisbon Port.* (Citeseer, 1998). at <http://citeseerx.ist.psu.edu/viewdoc/download?doi=10.1.1.453.4717&rep=rep1&type=pdf>

48. Moore, R. H., Thornhill, K. L., Weinzierl, B., Sauer, D., D'Ascoli, E., Kim, J., Lichtenstern, M., Scheibe, M., Beaton, B., Beyersdorf, A. J., Barrick, J., Bulzan, D., Corr, C. A., Crosbie, E., Jurkat, T., Martin, R., Riddick, D., Shook, M., Slover, G., Voigt, C., White, R., Winstead, E., Yasky, R., Ziemba, L. D., Brown, A., Schlager, H. & Anderson, B. E. Biofuel blending reduces particle emissions from aircraft engines at cruise conditions. *Nature* **543,** 411–415 (2017).

49. Burkhardt, U. & Kärcher, B. Global radiative forcing from contrail cirrus. *Nat. Clim. Change* **1,** 54–58 (2011).